JOURNAL OF GEOPHYSICAL RESEARCH, VOL. 96, NO. C7, PAGES 12,781–12,795, JULY 15, 1991

Wave Variance Partitioning in the Trough of a Barred Beach

PETER A. HOWD, JOAN OLTMAN-SHAY,[1] AND ROBERT A. HOLMAN

College of Oceanography, Oregon State University, Corvallis

The wave-induced velocity field in the nearshore is composed of contributions from incident wind waves ($f > 0.05$ Hz), surface infragravity waves ($f < 0.05$ Hz, $|\kappa| < (\sigma^2/g\beta)$) and shear waves ($f < 0.05$ Hz, $|\kappa| > \sigma^2/g\beta$), where f is the frequency, $\sigma = 2\pi f$, κ is the radial alongshore wavenumber ($2\pi/L$, L being the alongshore wavelength), β is the beach slope, and g is the acceleration due to gravity. Using an alongshore array of current meters located in the trough of a nearshore bar (mean depth ≈ 1.5 m), we investigate the bulk statistical behaviors of these wave bands over a wide range of incident wave conditions. The behavior of each contributing wave type is parameterized in terms of commonly measured or easily predicted variables describing the beach profile, wind waves, and current field. Over the 10-day period, the mean contributions (to the total variance) of the incident, infragravity, and shear wave bands were 71.5%, 14.3% and 13.6% for the alongshore component of flow (mean rms oscillations of 44, 20, and 19 cm s^{-1}, respectively), and 81.9%, 10.9%, and 6.6% for the cross-shore component (mean rms oscillations of 92, 32, and 25 cm s^{-1}, respectively). However, the values varied considerably. The contribution to the alongshore (cross-shore) component of flow ranged from 44.8–88.4% (58.5–95.8%) for the incident band, to 6.2–26.6% (2.5–32.4%) for the infragravity band, and 3.4–33.1% (0.6–14.3%) for the shear wave band. Incident wave oscillations were limited by depth-dependent saturation over the adjacent bar crest and varied only with the tide. The infragravity wave rms oscillations on this barred beach are best parameterized by the offshore wave height, consistent with previous studies on planar beaches. Comparison with data from four other beaches of widely differing geometries shows the shoreline infragravity amplitude to be a near-constant ratio of the offshore wave height. The magnitude of the ratio is found to be dependent on the Iribarren number, $\xi_0 = \beta(H/L_0)^{-1/2}$. Shear waves are, as previous observation and theory suggest (Oltman-Shay et al., 1989; Bowen and Holman, 1989), significantly correlated with a prediction of the seaward facing shear of the longshore current.

INTRODUCTION

Motivation

For nearly two decades, one of the primary interests in the study of nearshore processes has been the characterization of two frequency bands of gravity waves: incident wind waves (0.33 Hz $> f >$ 0.05 Hz) and infragravity waves ($f <$ 0.05 Hz). The recent discovery of a third "band," shear waves [*Oltman-Shay et al.*, 1989*a*; *Bowen and Holman*, 1989], has added a new twist to the difficult problem of quantifying wave energy in the nearshore.

This paper has two primary objectives: (1) to provide an overview of the variance contributions of these different waves in the trough of a barred beach (the contribution of shear waves, which has not been previously quantified, is of particular interest) and (2) to examine the lowest-order controls of variance on a barred beach and to compare our findings with those of previous studies. In the remainder of this section we will review some of the relevant literature concerning the three wave types and their behaviors in the surf zone. We then discuss the acquisition and analysis techniques for the present data, followed by the presentation of our findings and a comparison with other field data.

Previous Work

It has been shown consistently that statistical measures of incident wind wave height become depth-limited in the inner surf zone of natural beaches, and thus independent of the offshore wave height, according to the linear relation

$$H_{\text{rms}} = \gamma h \tag{1}$$

where $H_{\text{rms}} = (8s^2)^{1/2}$, s^2 is the incident wave variance, and h is the local water depth. For monochromatic laboratory waves, *Galvin and Eagleson* [1965] found γ to have a value ranging from 0.7 to 1.2. For field data, *Thornton and Guza* [1982] found γ to be much lower, approximately 0.42. Many researchers have reported γ to be a function of beach slope and/or wave steepness [*Bowen et al.*, 1968; *Weishar and Byrne*, 1978; *Sallenger and Holman*, 1985*b*]. Statistical representations of random waves from field experiments include both broken and unbroken waves, one reason why the saturation value of γ is significantly lower for field data than for monochromatic laboratory waves.

Infragravity waves are traditionally considered to be those surface gravity waves which result from the second-order interaction of incident wind waves. Under most conditions in surf zones on coasts open to the ocean, these waves have frequencies ranging from 0.005 to 0.05 Hz. The free infragravity waves can be broken into two distinct groups: a discrete set of edge wave modes, which are trapped to the shoreline, and a continuum of leaky waves, which reflect from the shoreline and radiate energy back out of the nearshore zone. Bounded waves, the forced displacement of the free water surface by the structure of wave groups [*Longuet-Higgins and Stewart*, 1964], also contribute to infragravity wave energy [*Guza et al.*, 1985; *Elgar and Guza*, 1985].

Edge waves on a plane beach of slope β have a discrete set of possible alongshore wavenumbers (κ), in the range $\sigma^2/g \le |\kappa| \le \sigma^2/g\beta$ satisfying the relationship $\sigma^2 = g|\kappa|\,(2n+1)\beta$ [*Eckart*, 1951], while for leaky waves there is a continuum with $|\kappa| < \sigma^2/g$ [*Suhayda*, 1974; *Guza and Bowen*, 1976]. Bound waves have no constraint on κ. Analytic solutions to the linear, shallow-water equations of motion on a plane-sloping beach give the free wave velocity potential (Φ) as

$$\Phi = ag/\sigma \cos(\kappa y - \sigma t)\, \phi(x) \tag{2}$$

where x is the cross-shore coordinate, y is the alongshore coordinate, and a is the wave amplitude at the shoreline [*Eckart*, 1951; *Suhayda*, 1974; *Guza and Bowen*, 1976]. The cross-shore nodal structure, $\phi(x)$, is as follows

[1]Now at Quest Integrated, Kent, Washington.

Paper number 91JC00434.
0148-0227/91/91JC-00434$05.00

$$\phi(x) = e^{-\kappa x} L_n(2\kappa x) \quad \text{edge waves}$$
$$\phi(x) = J_0\left(\frac{4\sigma^2 x}{g\beta}\right)^{1/2} \quad \kappa = 0 \quad \text{leaky wave} \tag{3}$$

with L_n being the Laguerre polynomial of order n (where n is the mode number of the edge wave) and J_0 is the zeroth-order Bessel function. The cross-shore structure of the higher-mode edge waves ($n > 2$) and the normally incident leaky wave are very similar near the shoreline and can be represented by the J_0 solution for approximate calculations [*Holman*, 1981; *Sallenger and Holman*, 1985*a*].

The cross-shore structure of infragravity waves has made frequency spectra of surf-zone currents difficult to interpret and compare between beaches. Wavenumber–frequency spectra estimated from cross-shore currents are also difficult to interpret, being dominated by some unresolved combination of high-mode edge waves, leaky waves, phase-locked edge waves, and bound waves [*Elgar and Guza*, 1985; *Oltman-Shay and Guza*, 1987; *Huntley*, 1988; *Haines and Bowen*, 1988]. However, wavenumber–frequency spectra of the alongshore component of currents have been shown to be particularly useful in determining the progressive low-mode edge wave content of the infragravity wave field [*Huntley et al.*, 1981; *Oltman-Shay and Guza*, 1987].

Past field studies have shown a dependence between the magnitude of the local infragravity wave oscillations, u_{IG} and a_{IG} (the cross-shore oscillation and the wave amplitude), and the offshore wind wave height [*Holman*, 1981; *Guza and Thornton*, 1985]. *Holman and Sallenger* [1985] and *Sallenger and Holman* [1985*a*] concluded that the dependence was also function of the deep-water Iribarren number, $\xi_0 = \beta/(H/L_0)^{1/2}$, where H and L_0 are representative of the deep-water height and wavelength of the incident waves, and of the dimensionless cross-shore distance, $\chi = \sigma^2 x/g\beta$, to the location of the measurements

$$u_{IG} = m_u(\chi, \xi_0)H \tag{4}$$

$$a_{IG} = m_a(\chi, \xi_0)H \tag{5}$$

where m is the slope of the linear regression.

Shear waves, a new class of nearshore wave, are distinguished by large wavenumbers, well outside the wavenumber range of gravity waves, $|k| > \sigma^2/g\beta$ [*Oltman-Shay et al.*, 1989*a*]. On the one beach studied to date, a typical energetic period is 200 s, with an alongshore wavelength of 200 m. This distinctive signature permits their contribution to total current variance to be separated in wavenumber–frequency space. *Bowen and Holman* [1989] show theoretically that these waves may be an instability of the mean longshore current which conserves potential vorticity. The

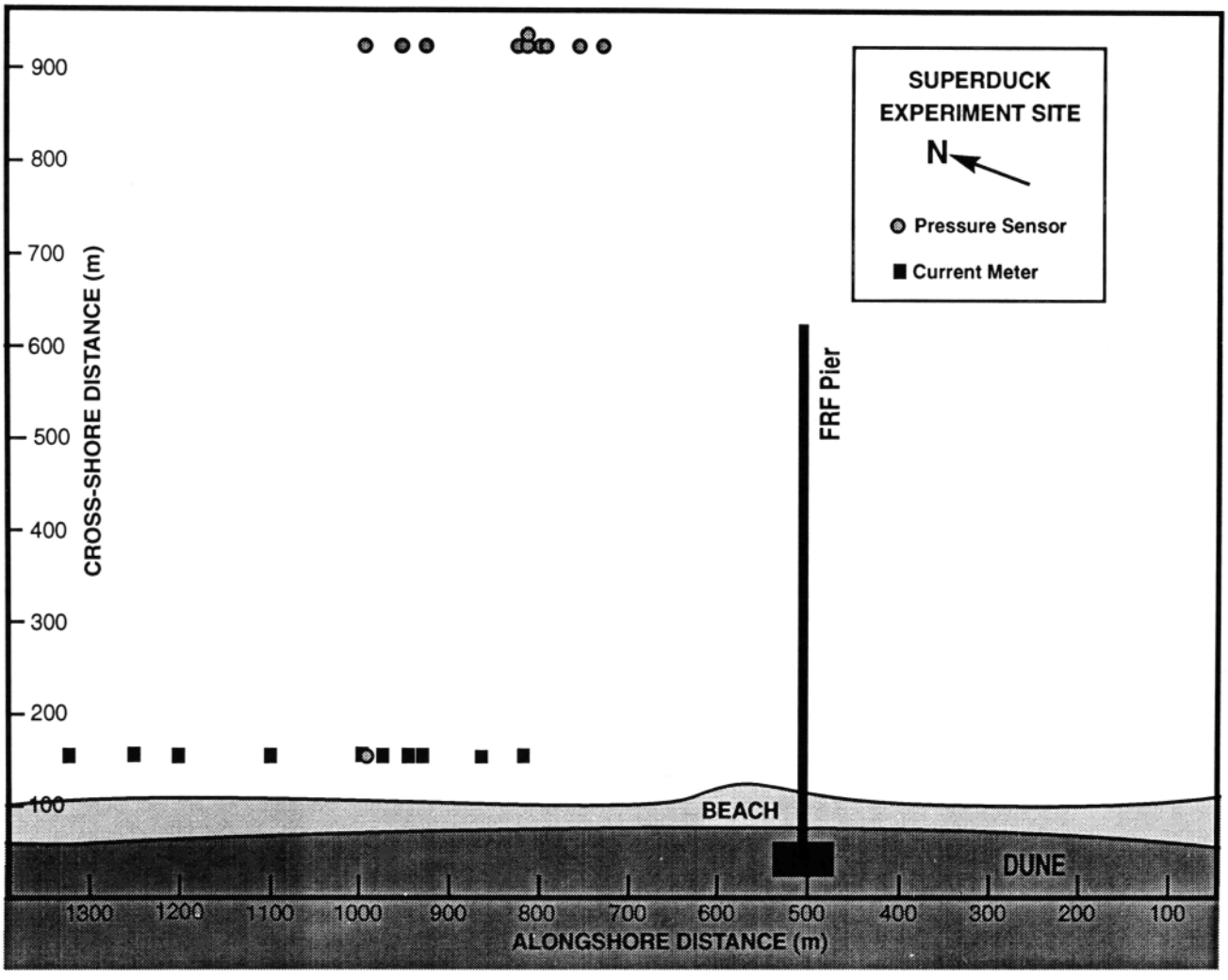

Fig. 1. Plan view of the SUPERDUCK field site at the Coastal Engineering Research Center's Field Research Facility in Duck, North Carolina. Shown are the nearshore current meter array, the nested pressure sensor, and the offshore wind wave directional array relative to the location of the pier. All measurements were made outside the known region of the pier's influence.

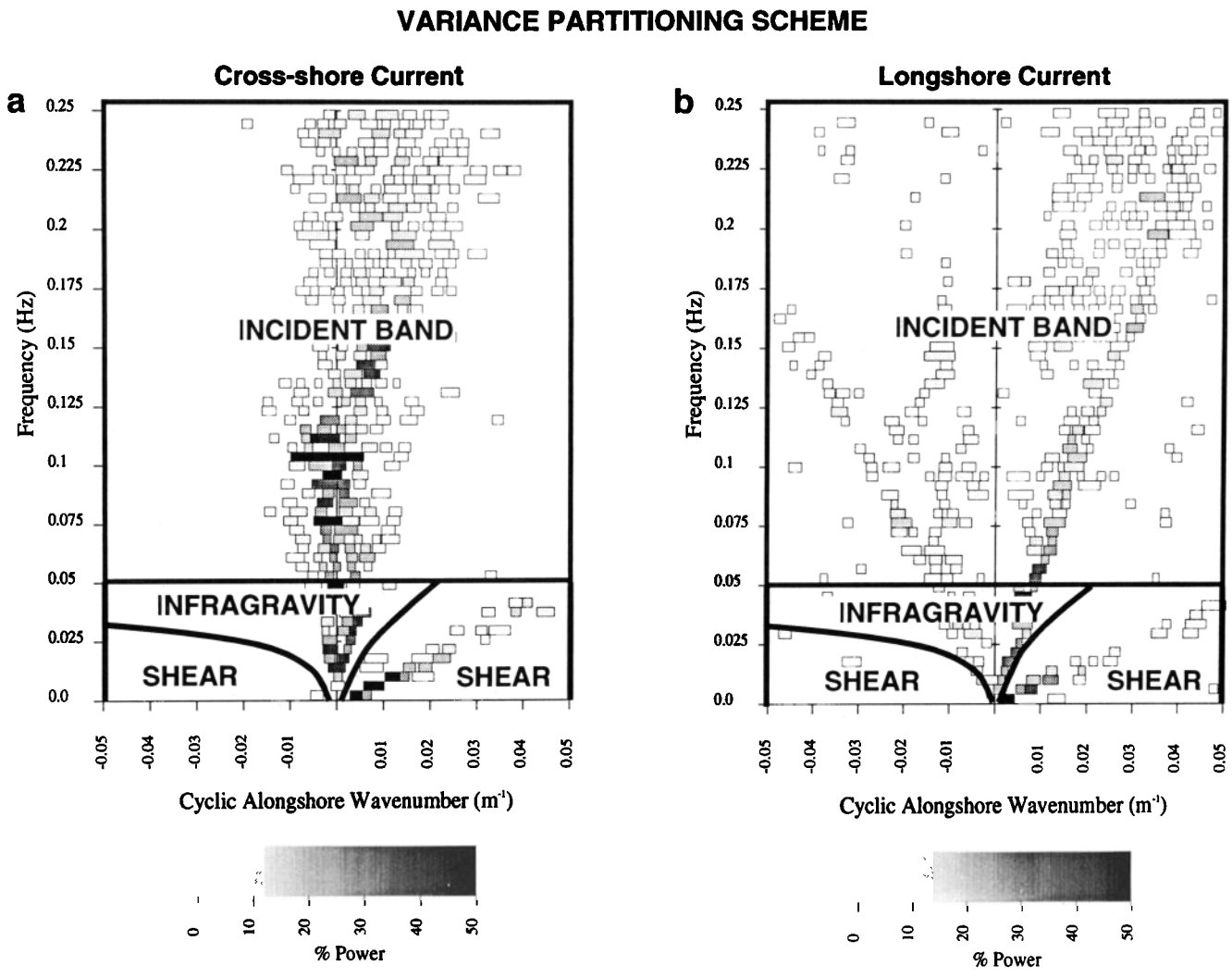

Fig. 2. Cyclic alongshore wavenumber ($k = 1/L$) versus frequency ($f = 1/T$) spectra, with lines showing the bounds of each of the three wave types. The boxes represent peaks in $S(k,f)$ with the darkness indicating the percent of variance in that frequency band contained in that peak. The width of the box indicates the half-power wavenumber bandwidth. The array was designrd for infragravity frequencies, thus the incident band is shown for reference only. (*a*). Estimate from cross-shore (u) current. (*b*). Estimate from longshore (v) current.

cross-shore shear of the mean longshore current provides the background vorticity (the role of Coriolis in larger-scale flows). Using a simple model, they show that there is a frequency range where a perturbation to the mean current (the shear wave) will grow exponentially at a rate which depends on the magnitude of the shear on the seaward face of the current ($\partial V/\partial x|_{seaward}$). While only the growth rate is predicted, we will test the assumption that the rms velocities of the shear waves also scale as the maximum seaward shear of the longshore current

$$u_{SW} = m_{SW} \left.\frac{\partial V}{\partial x}\right|_{seaward} \quad (6)$$

METHODS

In this section we briefly describe the field site, the instrumentation used in this study, and the data sampling. Then we present the analysis techniques and the sensitivity of these techniques to different processing options.

The data used for this study were collected as part of the SUPERDUCK experiment [*Crowson et al.*, 1988] hosted by the Coastal Engineering Research Center (CERC) Field Research Facility (FRF) in Duck, North Carolina, during October, 1986 (Figure 1). The beach is located near the center of a 100-km-long barrier island. The mean slope is approximately 1 in 10 on the foreshore, decreasing offshore to 1 in 100. Sand bars are consistently present, most commonly in a 3-dimensional configuration which becomes linear during most storm events [*Lippmann*, 1989]. The extreme tide range during the experiment was 137 cm.

An array of 10 Marsh-McBirney bidirectional electromagnetic current meters was deployed approximately 55 m seaward of the mean shoreline position in the trough of a nearshore bar system. The depth ranged from ~0.5 to ~2.5 m over the course of this study. Only the seven southernmost sensors were used in this study to minimize spatial inhomogeneity. The sampled array was thus 290 m in length, sufficient to resolve typical wavelengths at this site [*Oltman-Shay et al.*, 1989*a*]. Sensors were oriented in such a manner that their axes coincided with the longshore ($+v$ currents flow north) and cross-shore ($+u$ currents flow offshore) directions. All gages remained submerged at low tide.

Complementary data were collected by other investigators. A

TABLE 1. Basic Environmental Conditions

Run	Day*	Time, EST	Tide	H, cm	T, s	α (°)	H_{INC}, cm	$\langle U \rangle$, cm s^{-1}	$\langle V \rangle$, cm s^{-1}
1	9	0930	high	57.8	6.4	−31.9		−4.5	16.3
2	9	2200	high	35.8	5.8	−29.9	19.6	2.8	3.6
3	10	1030	high	184.2	7.3	24.3	53.5	31.5	−159.3
4	10	1700	low	205.5	7.9	16.0	36.4	12.9	−114.4
5	10	2320	high	216.5	8.9	8.9	55.8	22.2	−88.1
6	11	0540	low	216.2	9.7	4.2	35.0	7.5	−52.7
7	11	1200	high	213.7	9.7	4.9	69.4	23.6	−41.3
8	11	1820	low	190.3	10.0	0.3	35.7	3.6	−13.0
9	12	0040	high	172.6	11.9	−3.7	61.3	14.4	30.5
10	13	0130	high	126.2	12.0	−10.4	57.2	16.4	29.1
11	14	1500	high	57.1	9.7	−25.3	49.6	4.8	21.4
12	15	0330	high	110.5	5.5	36.1	63.3	8.9	−87.1
13	15	0945	low	96.2	6.0	25.0	23.3	5.9	−91.1
14	15	1600	high	71.3	6.4	22.7	49.8	5.0	−35.5
15	15	2200	low	71.4	4.4	25.8	20.2	2.8	−64.2
16	16	0400	high	79.3	4.6	27.9	50.5	5.0	−40.0
17	16	1630	high	75.8	5.2	24.4	45.3	4.9	−35.3
18	16	2240	low	69.1	5.5	16.5	21.4	3.8	−52.8
19	17	0450	high	75.5	5.1	18.4	48.5	5.2	−29.5
20	17	1100	low	70.1	5.8	6.6	21.4	3.7	−40.7
21	18	0530	high	91.3	9.7	20.4	51.8	9.6	−45.3

H, incident root mean square wave height in 8-m depth; T, peak spectral period in 8-m water depth, α, median spectral direction in 8-m water depth (CCW from shore normal); H_{INC}, incident root mean square wave height in the surf zone (from pressure); $\langle U \rangle$, mean cross-shore current averaged over the array of current meters; $\langle V \rangle$, mean longshore current averaged over the array of current meters.

*Day of the month October 1986.

pressure sensor (maintained by Asbury Sallenger, Jr., U.S. Geological Survey) was located 3 m south of the central current meter. The wind wave climate was sampled in 8-m depth, using a 255-m-long array of bottom-mounted pressure sensors as part of the routine monitoring program of the FRF. The surf-zone morphology was measured using the FRF Coastal Research Amphibious Buggy (CRAB) [*Birkemeier and Mason*, 1984].

All current meters and pressure sensors were hard-wired to the data collection system. Gages were sampled at 2 Hz for 4 hours centered on high and low tides. High-quality data from the majority of the gages were collected for 10 days, with the exception of approximately 22 hours lost owing to a power failure. Each time series was exhaustively checked for reliability in both time and frequency domains. Suspect gages were excluded from further analysis, as were time periods marked by large spatial inhomogeneities or temporal nonstationarity. From a total of 36 collections, 21 were processed further.

The current meter array data were used to calculate the alongshore wavenumber–frequency spectra for both the cross-shore and alongshore components of flow. First, each of the 21 time series was divided into 13 ensembles with 50% overlap, 2048 s in length, demeaned and then detrended (using a least squares quadratic fit) prior to being tapered with a Kaiser-Bessel window. Wavenumber–frequency spectra were estimated using the iterative maximum likelihood estimator (IMLE) developed by *Pawka* [1982, 1983] and previously applied to surf-zone data by *Oltman-Shay and Guza* [1987] and *Oltman-Shay et al.* [1989*a*].

Variance for each 4-hour run was then partitioned between the three bands in wavenumber–frequency space (Figure 2). Integrated variances for each band were given by

$$s^2_{INC} = \int_{0.05}^{0.33} \int_{-\kappa_{NY}}^{+\kappa_{NY}} S(\kappa, f)\, d\kappa\, df \quad (7)$$

$$s^2_{IG} = \int_{0}^{0.05} \int_{(-\kappa_0-\delta)}^{(+\kappa_0+\delta)} S(\kappa, f)\, d\kappa\, df \quad (8)$$

$$s^2_{SW} = \int_{0}^{0.05} \int_{-\kappa_{NY}}^{+\kappa_{NY}} S(\kappa, f)\, d\kappa\, df - s^2_{IG} \quad (9)$$

where s^2 is the integrated variance for each of the bands, κ_{NY} is the Nyquist radial wavenumber of the array, $\pm\kappa_0$ are the estimated mode zero wavenumbers, δ is a constant wavenumber offset used to account for the wavenumber bandwidth of the mode zero

TABLE 2. Basic Statistics

Variable	Mean	S.D.	Maximum	Minimum
		Offshore		
H_{rms}, cm	118.4	61.1	216.5	35.8
T, s	7.5	2.3	12.0	4.4
α, °	−8.3	19.1	6.1	−31.9
		Surf-Zone		
H_{INC}, cm	43.5	15.4	69.4	19.6
u_{INC}, cm s^{-1}	92.0	11.0	108.5	74.2
u_{IG}, cm s^{-1}	32.1	16.0	62.5	15.0
u_{SW}, cm s^{-1}	25.1	10.6	40.6	6.0
v_{INC}, cm s^{-1}	44.4	8.8	60.8	27.5
v_{IG}, cm s^{-1}	20.2	7.8	32.6	8.4
v_{SW}, cm s^{-1}	19.5	7.3	34.8	8.4
% u_{INC}	81.9	11.8	95.8	58.5
% u_{IG}	10.9	8.5	32.4	2.5
% u_{SW}	6.6	4.1	14.3	0.6
% v_{INC}	71.5	11.2	88.4	48.8
% v_{IG}	14.3	6.0	26.6	6.2
% v_{SW}	13.6	6.7	33.1	3.4

Mean indicates mean value of variable for the 21 data runs, S.D. is standard deviation about mean value, Maximum is maximum value of variable for these 21 runs, Minimum is minimum value of variable for these 21 runs. The mean value for each run is the result of an average of many sensors, with the exception of H_{INC}, which is calculated from a single pressure gage.

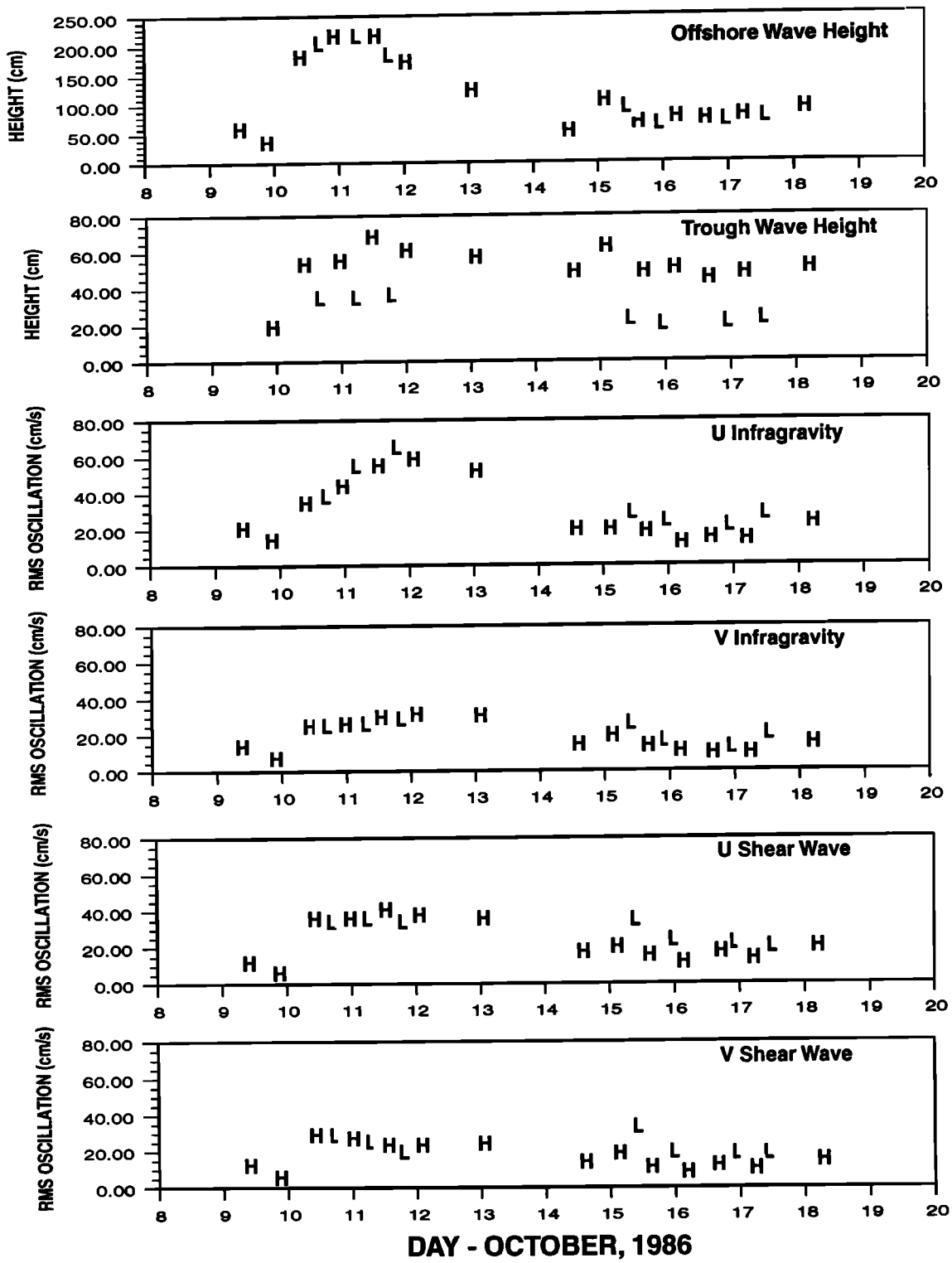

Fig. 3. Time series of 4-hour mean statistics for wave parameters at the offshore array pressure sensors and for the current meters/pressure sensor in the surf zone. H and L refer to the tide stage. See the text for details of how the variances were partitioned between wave types.

spectral peak (set at 0.0094 m^{-1} in radial units; this accounts for the variation in κ from the bottom of the frequency bin to the top, see *Oltman-Shay and Guza* [1987]) and $S(\kappa,f)$ is the spectral density. The subscripts refer to the incident (INC), infragravity (IG), and shear wave (SW) bands, respectively.

The incident band integration limits (in frequency) were chosen based on the spectral characteristics of the offshore pressure gage array data. The upper limit, 0.33 Hz, was the highest frequency for which the depth-attenuated wave signals reliably exceeded instrument noise. The lower limit (0.05 Hz) was chosen such that all wind wave variance would be excluded from estimates of the infragravity motions (but not the opposite). Examination of

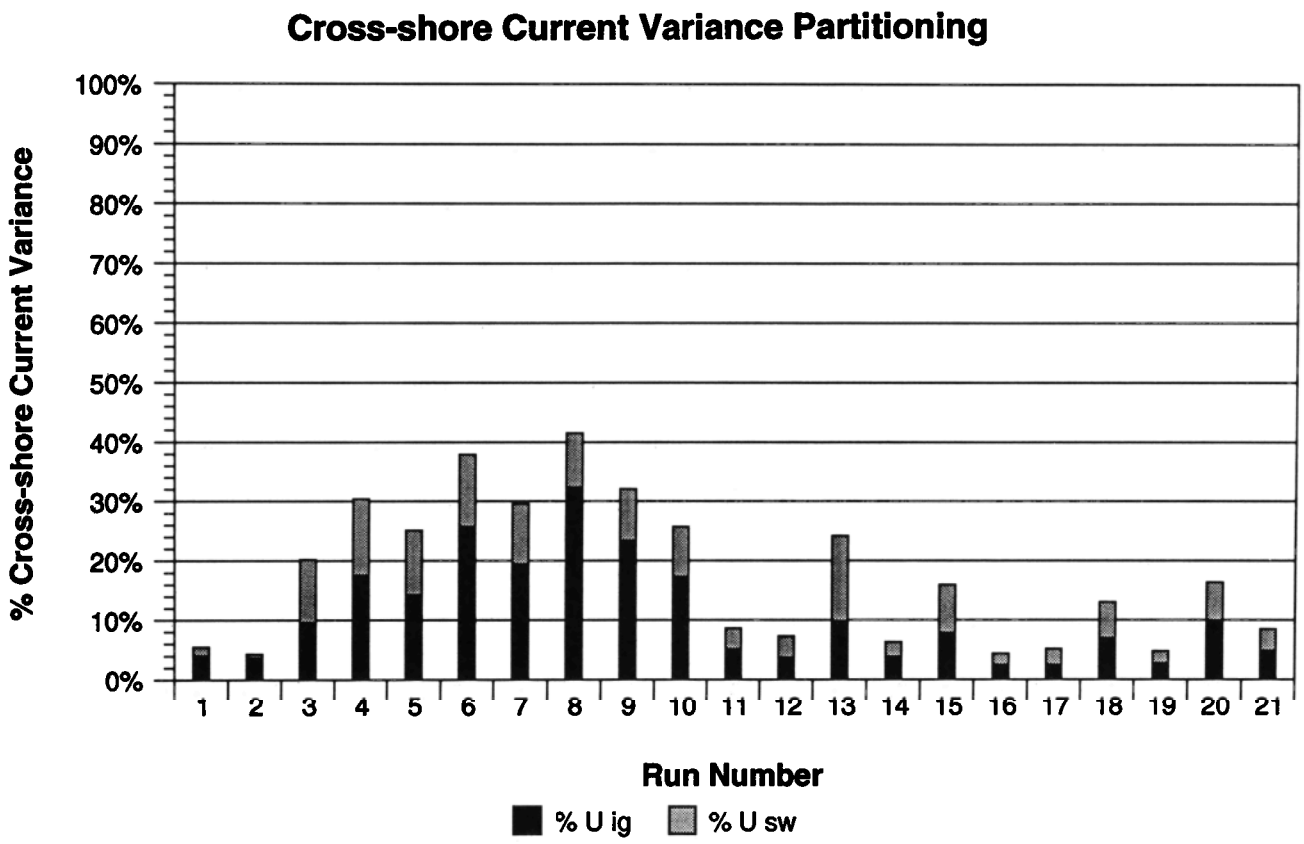

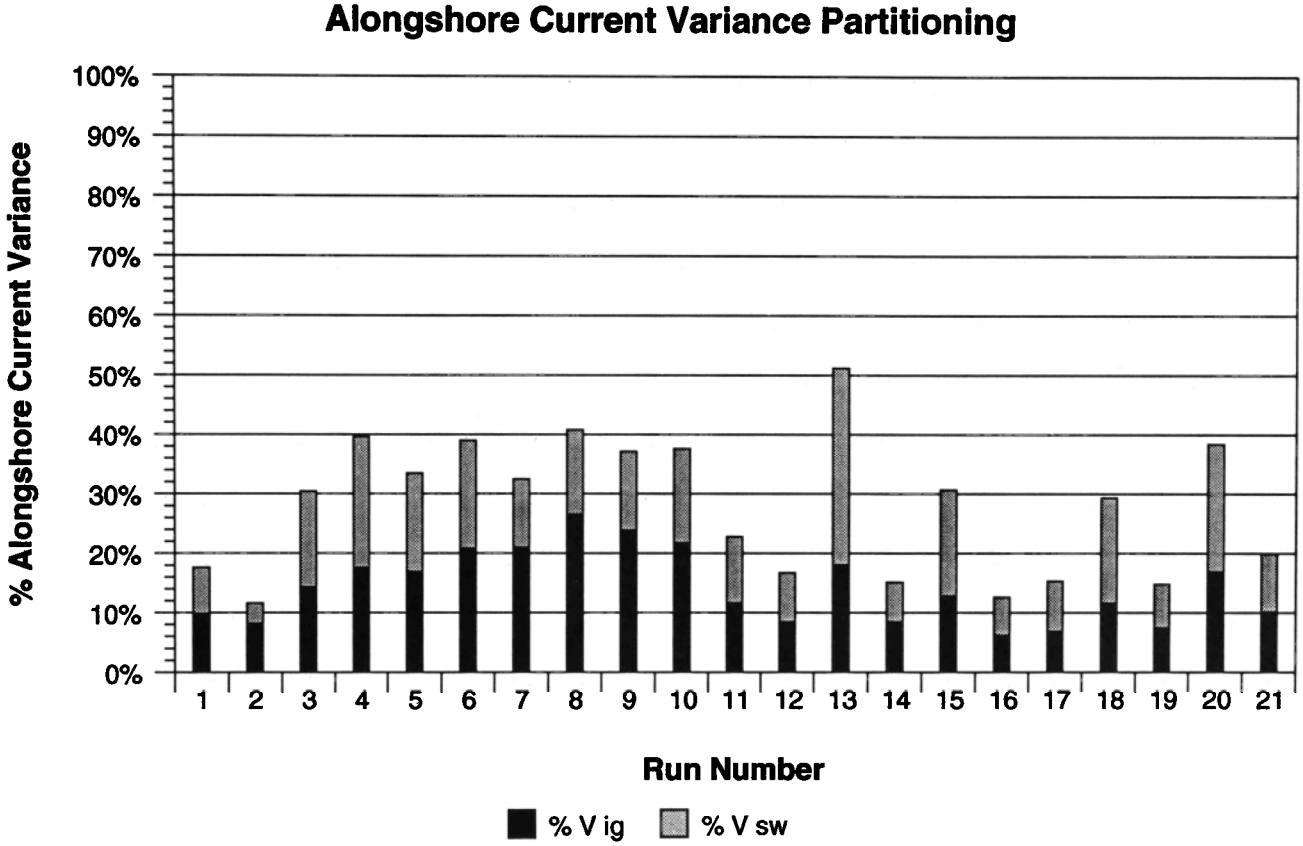

Fig. 4. The percent contributions made by each band to the total variance of each flow component (the incident band contribution brings the total to100%). The incident band is clearly dominant at this cross-shore location for both the alongshore and cross-shore flows.

TABLE 3. Regression Results

Y	X	$m \pm 95\%$ Confidence	b	r^2*
H_{INC}	H_{rms}	0.100 ± 0.111	31.3	0.158
H_{INC}	tide	0.261 ± 0.063	30.0	0.798
u_{IG}	H_{rms}	0.224 ± 0.064	5.6	0.729
v_{IG}	H_{rms}	0.110 ± 0.030	7.1	0.746
% u_{IG}	H_{rms}	0.001 ± 0.0004	-0.023	0.641
% v_{IG}	H_{rms}	0.059 ± 0.001	0.007	0.526
u_{SW}	$\|V\|$	0.143 ± 0.117	17.7	0.245
v_{SW}	$\|V\|$	0.130 ± 0.071	12.7	0.419
% u_{SW}	$\|V\|$	0.0007 ± 0.0004	0.032	0.342
% v_{SW}	$\|V\|$	0.0009 ± 0.0007	0.088	0.260
u_{SW}	$\partial V_M/\partial x$	868.7 ± 388.9	13.9	0.521
v_{SW}	$\partial V_M/\partial x$	637.7 ± 249.2	11.2	0.587
% u_{SW}	$\partial V_M/\partial x$	3.491 ± 1.457	0.021	0.555
% v_{SW}	$\partial V_M/\partial x$	4.172 ± 2.981	0.083	0.300

Here (19 DOF) $Y = mX + b$ + error.

*The r^2 is greater than 0.185 correlation different from 0 at 95% level, and r^2 is greater than 0.303 correlation different from 0 at 99% level.

spectra from the 8-m array showed no energetic swell at frequencies below 0.05 Hz. The 0.05-Hz cutoff results in a small underestimate of the infragravity band variance.Varying the cutoff from 0.04 to 0.06 Hz resulted in typical changes of ±5% of the total variance, with the trade always being between incident and infragravity regimes. The results were not sensitive to reasonable choices for δ.

The wavenumber limits for the infragravity band calculation are based on estimates of $\pm\kappa_0$, the largest wavenumbers possible for free surface gravity waves (plus and minus signs indicate direction of propagation). We have assumed $\pm\kappa_0$ can be closely approximated by the plane beach solution with a simple correction for the mean longshore current

$$\pm\kappa_0 = \frac{[\sigma - (\pm\kappa_0)\, V]^2}{g\beta} \tag{10}$$

Kenyon [1972] demonstrated that the dispersion curve for the mode zero edge wave, in the presence of a current with constant shear, behaves as if it were Doppler-shifted, as above, by the longshore current at an offshore distance of $L/4\pi$, which is approximately 33 m for the "typical" mode zero edge wave in this study. This behavior has also been reported by *Oltman-Shay and Guza* [1987] for field data. Values chosen for the beach slope and mean longshore current at $x = 33$ m were based on average values over the length of the alongshore array. A constant β was chosen to match the observed mode zero dispersion lines.

Tests were conducted concerning the sensitivity of the analysis to different data windows and ensemble length, detrending, and changes in the wavenumber–frequency partitioning scheme. There were no statistically significant differences from varying the ensemble and window characteristics. As expected, detrended

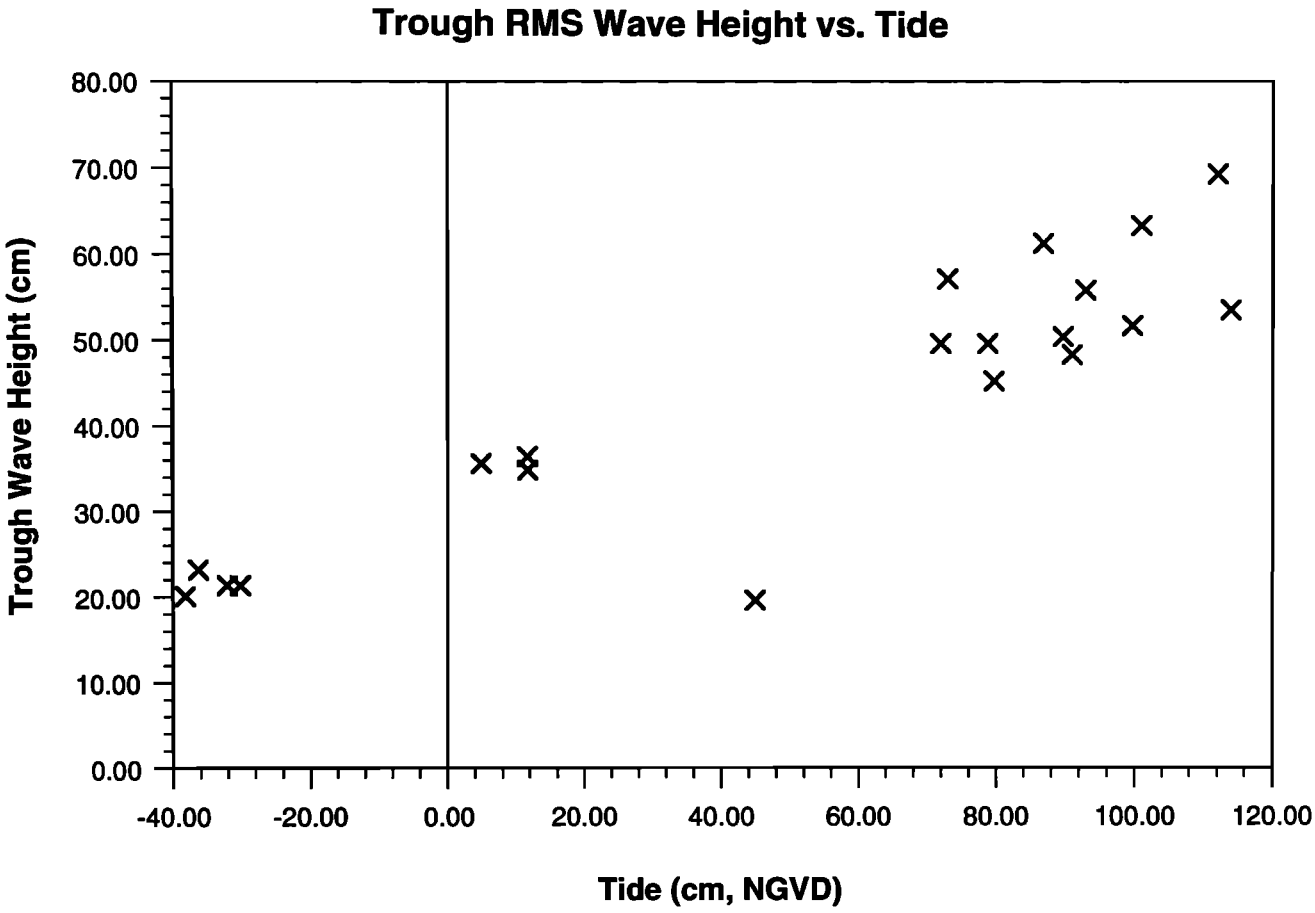

Fig. 5. The magnitude of the incident band rms wave height measured in the trough plotted versus the tide elevation. This, combined with the lack of correlation between offshore wave height and rms oscillation, indicates the incident band is depth-limited during the majority of the experiment. The one outlier represents our lowest wave conditions (2200 EST on October 9), when oscillations were not depth-limited.

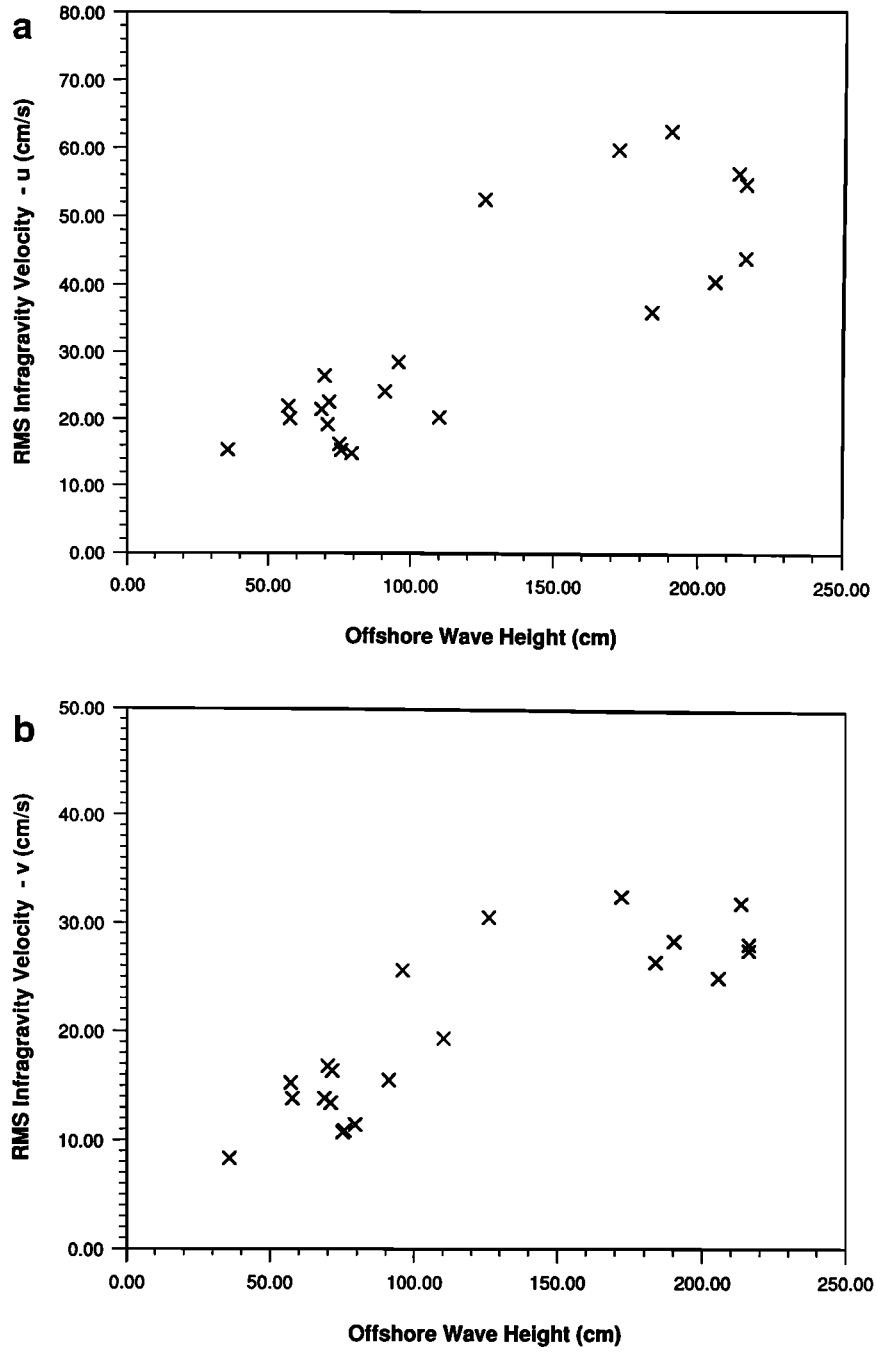

Fig. 6. Values of (*a*) u_{IG} and (*b*) v_{IG} plotted versus the offshore wave height, H_{rms}. Both show a linear relationship with increasing wave height, as has been seen on other beaches.

data contained less total variance than data with trends, but the differences occurred only in the lowest-frequency bin.

Results

Statistics

Tables 1 and 2 and Figures 3 and 4 present a summary of basic wave and current statistics. In all cases, the root mean square (rms) statistics, calculated as $(8s^2)^{1/2}$, are presented for wave heights and current oscillations. Because of the processing techniques, rms current oscillations represent the average over the array. Percent contributions always refer to the percent of total variance contributed by the band.

The data cover a wide range of conditions, with H_{rms} in 8-m water depth ranging from 30 cm to over 215 cm (significant heights in excess of 300 cm), the peak period varying from 4.4 to 12.0 s, and the mean longshore current averaged over the current meter array, $\langle V \rangle$, ranging from −159 cm s^{-1} (southward) to +31 cm s^{-1} (northward).

Statistics for the rms oscillations in each band are found in Table 2. Mean values (plus or minus one standard deviation) over the experiment for u_{INC} and v_{INC} are 92 ± 11 cm s^{-1} and 44 ± 9 cm s^{-1}, with maxima of 108 and 61 cm s^{-1}, respectively. Mean values of the u and v infragravity wave oscillations (u_{IG} and v_{IG}) were 32.1 ± 16.0 cm s^{-1} and 20.2 ± 7.8 cm s^{-1}, with maxima of

TABLE 4. Iribarren Regression Results

Y	X	$m \pm 95\%$ Confidence	b	r^2*
u_{IG} ($\xi_0 < 0.40$)	ξ_0	0.157 ± 0.054	8.26	0.808
u_{IG} ($\xi_0 > 0.40$)	ξ_0	0.256 ± 0.076	6.14	0.872
v_{IG} ($\xi_0 < 0.40$)	ξ_0	0.093 ± 0.046	8.00	0.677
v_{IG} ($\xi_0 > 0.40$)	ξ_0	0.121 ± 0.043	7.00	0.819

Here (8 DOF) $Y = mX + b$ + error.
*The r^2 is greater than 0.400 correlation different from 0 at 95% level, and r^2 is greater than 0.585 correlation different from 0 at 99% level.

TABLE 5. Directional Dependence

Y	X	$m \pm 95\%$ Confidence	b	r^2	Mean Square Error
u_{IG}					
	H_{rms} alone	0.22 ± 0.06	5.62	0.73	76.70
	H_{rms}	0.14 ± 0.06			
	$\lvert\alpha\rvert$	-0.74 ± 0.38			
			28.80	0.85	43.38
v_{IG}					
	H_{rms} alone	0.11 ± 0.02	7.14	0.75	17.08
	H_{rms}	0.10 ± 0.04			
	$\lvert\alpha\rvert$	-0.14 ± 0.24			
			11.44	0.76	16.74

Here $Y = m_1X_1 + m_2X_2 + b$ + error.

62.5 and 32.6 cm s^{-1}, respectively. The mean shear wave oscillations were 25.1 ± 10.6 cm s^{-1} for u_{SW} and 19.5 ± 7.3 cm s^{-1} for v_{SW}. Maxima were 41 and 35 cm s^{-1}, respectively.

The percentage contributions of each band to the total variance are shown in Figure 4. The incident band oscillations, on average, provided 71.5% of the alongshore current variance and 81.9% of the cross-shore current variance. The percent contribution of the infragravity band waves ranged from 6.2% to 26.6% of the longshore variance and from 2.5% to 32.4% of the cross-shore variance at the surf-zone location of the alongshore array. Shear wave oscillations contributed up to 33.1% of the total longshore current variance, but only up to 14.3% of the cross-shore variance.

Parameterization

Incident band rms current oscillations, u_{INC} and v_{INC}, and wave heights, H_{INC}, in the bar trough were observed to be depth-limited, but not saturated, in agreement with the previous observations of *Wright et al.* [1986]. However, there was evidence for saturation seaward of the array, as there was a lack of statistically significant correlations between the incident wave heights in the trough and the offshore wave height (Table 3). The oscillations were, however, significantly correlated with the tide (Table 3, Figure 5), clearly showing that the incident band was typically limited by depth, presumably at the bar crest. Given that the surf-zone instruments were in the trough of the nearshore bar for much of the experiment, it is no surprise that the local mean value of γ (0.20 ± 0.03) was considerably lower than saturation value (0.30 ± 0.01) previously predicted for this beach at the bar crest [*Sallenger and Holman*, 1985*b*].

Values of u_{IG}, v_{IG}, and their percent contributions, were found to be significantly correlated with the offshore wave height (Figures 6*a* and 6*b*), in agreement with current meter data from similar water depths on three other beaches [*Holman*, 1981; *Guza and Thornton*, 1985]. Comparison with these data sets will be presented in the discussion. *Holman and Sallenger* [1985] and *Guza et al.* [1985] also found that for the infragravity band, the slopes of the regression lines for swash amplitude versus offshore wave height depended on the Iribarren number (larger slopes for larger ξ_0). To test this dependence for the velocity oscillations, we have divided the data set into two subsets ($\xi_0 < 0.40$ and $\xi_0 > 0.40$) and calculated the regression slope for each group (Table 4). While there is an increase in slope for the higher ξ_0, the difference is not statistically significant for this small sample.

The large range of conditions experienced during SUPERDUCK also allowed examination of the impact of the wind wave incident angle on infragravity band variance levels.

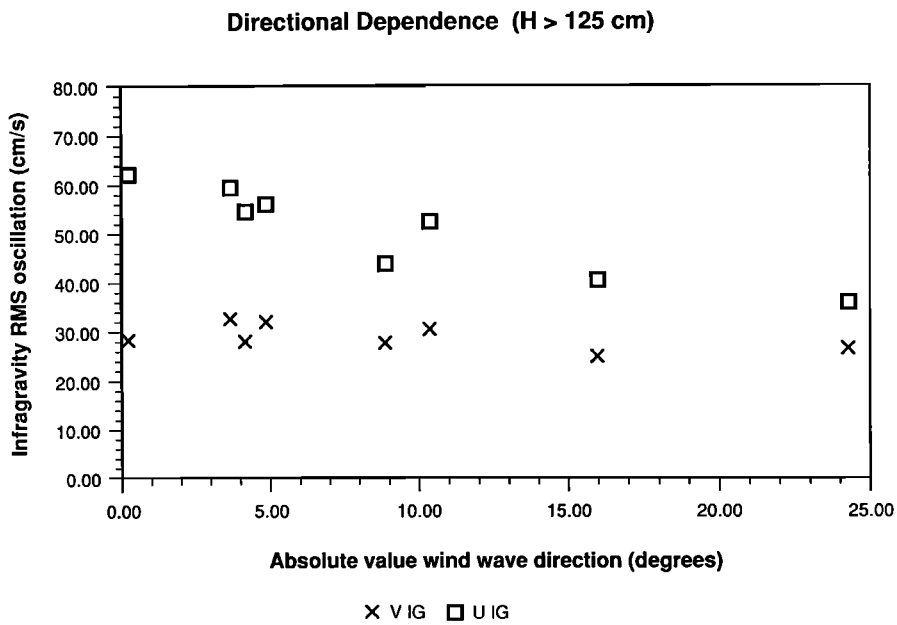

Fig. 7. The dependence of rms infragravity oscillations on the absolute value of the incident direction, $\lvert\alpha\rvert$, for cases with $H_{rms} >$ 125 cm.

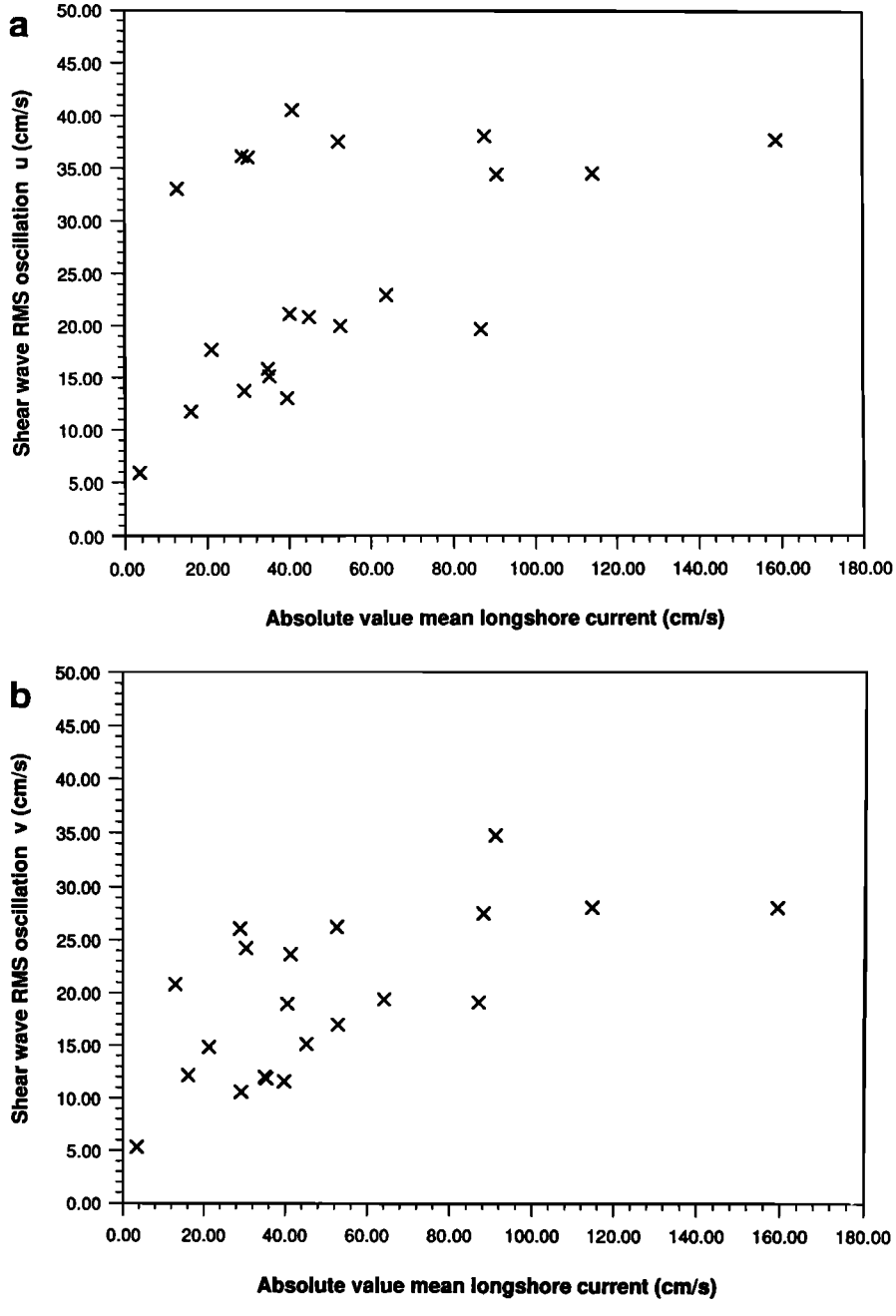

Fig. 8. Values of (*a*) u_{SW} and (*b*) v_{SW} plotted versus the absolute value of the measured mean longshore current, $|\langle V \rangle|$.

Multiple regression analysis shows a significant negative relation between u_{IG} and $|\alpha|$, while there is not a significant relationship between v_{IG} and $|\alpha|$ (Table 5). The directional dependence is most clearly illustrated (Figure 7) during the passage of the storm (October 10–12), when the direction of wave approach was highly variable, but the wave height was nearly constant. The u_{IG} oscillations clearly decrease as $|\alpha|$ increases, while the v_{IG} oscillations are essentially constant. Preliminary analysis suggests that u_{IG} oscillations in the presence of a large $|\alpha|$ (low u_{IG}) are dominated by high-mode edge waves, while the low $|\alpha|$ u_{IG} oscillations are dominated by more energetic leaky or bound waves [*Elgar et al.*, 1989; *Oltman-Shay et al.*, 1989*b*].The v_{IG} oscillations are expected to be dominated by low-mode edge waves regardless of the leaky/high-mode contributions to u_{IG}.

Shear waves are hypothesized to scale with the longshore current shear (equation (5)), but no measurements of the longshore current shear were obtained for extended periods of the experiment. Thus based on the observations of *Oltman-Shay et al.* [1989*a*], we assume that the absolute value of the measured mean longshore current, $|\langle V \rangle|$, is a proxy for the dynamically important shear (Figures 8*a* and 8*b*). The mean current, $\langle V \rangle$, was estimated as the mean of the 4-hour averages of the current meters used in the wavenumber–frequency spectral analysis. The u_{SW} and v_{SW} were significantly correlated with $|\langle V \rangle|$, but with considerable scatter.

In an attempt to better parameterize the shear waves, we have modeled the longshore current, and its theoretically important shear, based on the work of *Thornton and Guza* [1983, 1986].

Wave heights in the surf zone were assumed to be Rayleigh-distributed with a probability (p) of

$$p(H) = \frac{2H}{H_{rms}} \exp\left[-\left(\frac{H}{H_{rms}}\right)^2\right] \quad (11)$$

This distribution is modified by a weighting function to provide a statistical estimate of those waves which are breaking. The mean dissipation due to wave breaking, $<\varepsilon>$ (integrated through the wave height distribution), is given by

$$<\varepsilon> = \left(\frac{3\pi^{1/2}}{16}\right)\rho g B^3 f \left(\frac{H_{rms}^5}{\gamma_{rms}^2 h^3}\right)\left\{1-\left[\frac{1}{\left(1-\left(\frac{H_{rms}}{\gamma_{rms} h}\right)^2\right)^{5/2}}\right]\right\} \quad (12)$$

where ρ is the density of water, B is an empirical coefficient representing the portion of the bore face actively breaking, and f is the peak incident frequency. It is then simple to step shoreward from the input conditions at the 8-m array, calculating wave height based on energy flux balance, with the incident angle varied according to Snell's law of linear wave refraction.

The wave height and dissipation profiles across the surf zone were then used to predict longshore current following *Thornton and Guza*, [1986]

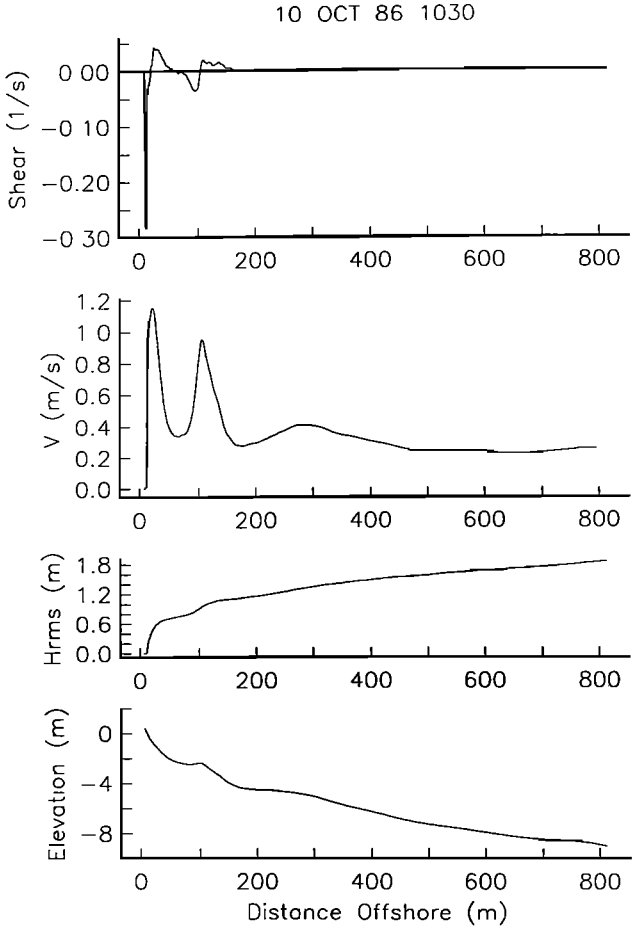

Fig. 9. Model results for H, V_M, and $\partial V_M/\partial x$ on the measured profile. The input values for H and α were those measured at the offshore array at the offshore boundary of the model. Two jets are seen in the current, one over the bar, and one at the shoreline. The shoreline jet is large owing to the assumption that all incident energy is dissipated (no reflection). Shear wave theory predicts that the shear on the seaward face of the bar is the dynamically important variable.

$$V_M(x) = \left\{\frac{\sin[\alpha(x)]}{\rho u(x)\, C(x)\, c_f}\right\} <\varepsilon> \quad (13)$$

where c_f is an empirical drag coefficient, $\alpha(x)$ is defined as by *Thornton and Guza* [1986], C is the phase velocity of the incident waves, and u is given for a Rayleigh distribution by

$$u(x) = \left[\frac{g}{4\pi h(x)}\right]^{1/2} H_{rms}(x) \quad (14)$$

We have assumed the bottom stress to be linear, ignored the turbulent Reynold's stresses, and assumed constant values for $\gamma = 0.45$, $B = 1.0$, and $c_f = 0.009$.

A typical output of the model is shown in Figure 9. The predicted maximum longshore current was significantly correlated with the observed current ($r^2 = 0.942$). We assume the model does a reasonable job of predicting the relative changes (between the 21 data collections) in the cross-shore structure of the longshore current in the absence of the mixing induced by the shear waves and Reynold's stresses. No attempt was made to further tune the model to match conditions observed in the surf zone.

The dependence of shear wave magnitude on the maximum of the modeled shear on the seaward face of the longshore current is shown in Figure 10. The correlations are not significantly improved over that with the mean velocity measured in the trough (Table 3). Clearly, more field data are needed to better define the forcing of this new phenomenon.

Discussion

The SUPERDUCK data, collected in the trough of a barred beach, have a "process signature" which qualitatively agrees with the results of *Wright and Short* [1983] and *Wright et al.* [1986]. They presented distinctive ratios between the different components of the flow field based on the morphodynamic state of the beach. The SUPERDUCK data clearly fall into the intermediate (long-shore bar and trough/rhythmic bar and beach) state between fully dissipative and fully reflective. The signature is characterized by low-frequency oscillations in the surf zone approximately half the magnitude of the incident band oscillations.

Four large data sets of u_{IG} oscillations and incident wave heights are available for quantitative comparison with the SUPERDUCK data. *Guza and Thornton* [1985] presented data from two experiments at two nonbarred beaches of very different slopes, Torrey Pines (TP) and Santa Barbara (SB). These data represent the variance integrated over the frequency range 0.005–0.05 Hz and averaged over a variable number of current meters positioned at depths between 1 and 2 m. The authors note that less than 10% of the energy lay at frequencies below 0.005 Hz. *Wright et al.* [1986] reported statistics for eight moderate- to high-energy ($H > 160$ cm) data runs of two–four sensors between 1- and 2-m depth (with highly variable cross-shore locations) from a barred section of Ninety Mile Beach in southeast Australia (AU). We chose one representative sensor for each data run (rather than average different cross-shore locations) and combined the subharmonic and infragravity bands (their infragravity band was $f < 0.03$ Hz). *Holman* [1981] presented data from a single sensor at 2-m depth, integrated from 0 to 0.05 Hz, on Martinique Beach (MA). The SUPERDUCK (SD) variances for this comparison include contributions from all wavenumbers in the frequency band 0–0.05 Hz. All data were converted to rms oscillations.

Figure 11*a* shows these five data sets of u_{IG} oscillations plotted versus offshore H. The four North American locations show sta-

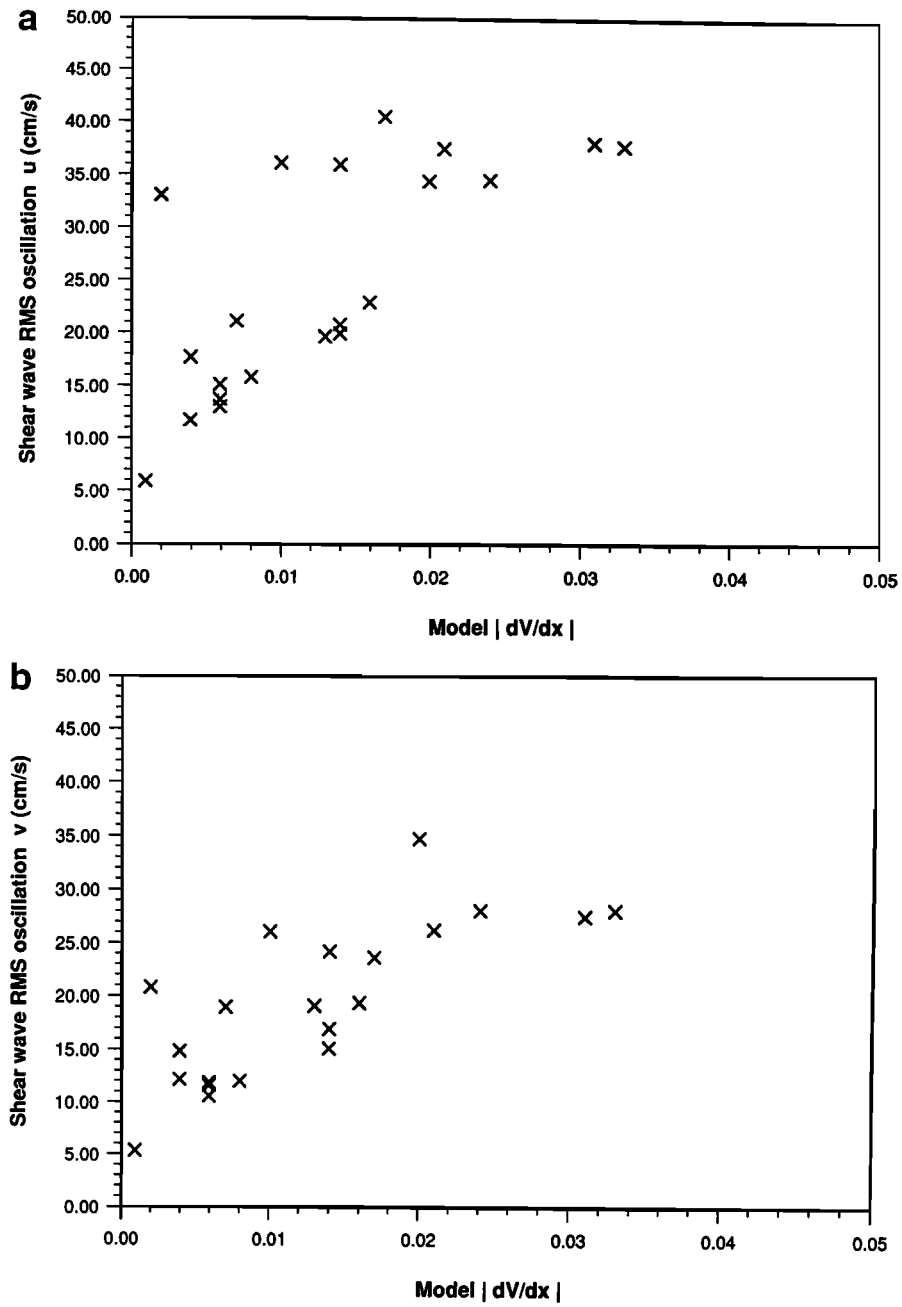

Fig. 10. Values of (*a*) u_{SW} and (*b*) v_{SW} plotted versus $|\partial V_M/\partial x|$, the absolute value of the modeled maximum current shear seaward of the bar crest. The scatter, of unknown origin, is not significantly reduced. Compare with Figure 11.

tistically significant positive regression slopes (Table 6) even while these slopes vary between the different beaches (except between TP and SB). This is reflected in the low skill (r^2) of linear regression models between u_{IG} and offshore H for the beaches as a group, but the high $r^2$for each beach individually. The regression slope for the Australian data is negative, a result of the highly variable cross-shore location of the chosen sensors (no one sensor was operational for all runs).

These results are not unexpected because infragravity waves have an offshore decay dependent on β. In an effort to remove complications arising from the cross-shore decay and varying instrument positions for the four data sets, we have calculated an "equivalent shoreline amplitude," $\hat{a}_{IG}$, by scaling the data from each beach by the predicted u_{IG} variance, s^2_{IGP}, contributed by a white shoreline spectrum of normally incident standing waves

$$s^2_{IGP} = \hat{a}^2_{IG} \int_0^{2\pi(0.05)} \int_0^{2\pi} \left\{ \frac{\partial}{\partial x} \left[\frac{g\cos(\sigma t)\,\phi(x_i)}{\sigma} \right] \right\}^2 dt\, d\sigma \quad (15)$$

where x_i is the instrument location and the point at which the derivative with respect to x is evaluated. This approach is very similar to that of *Sallenger and Holman* [1985*a*]. Assuming a white spectrum allows $\hat{a}^2_{IG}$ to be taken outside the integrals. We assume that the cross-shore shape, $\phi(x)$, can be represented by the leaky wave solution given in (3). Substitution and solution for $\hat{a}^2_{IG}$ yields

$$\hat{a}^2_{IG} = \frac{\int_0^{2\pi(0.05)} S(\sigma)\, d\sigma}{\int_0^{2\pi(0.05)} \int_0^{2\pi} \left\{ \frac{\partial}{\partial x} \left[g\cos(\sigma t)\, J_0\left(\left(\frac{4\sigma^2 x}{g\beta} \right)^{1/2} \right) \right] \right\}^2 dt\, d\sigma} \quad (16)$$

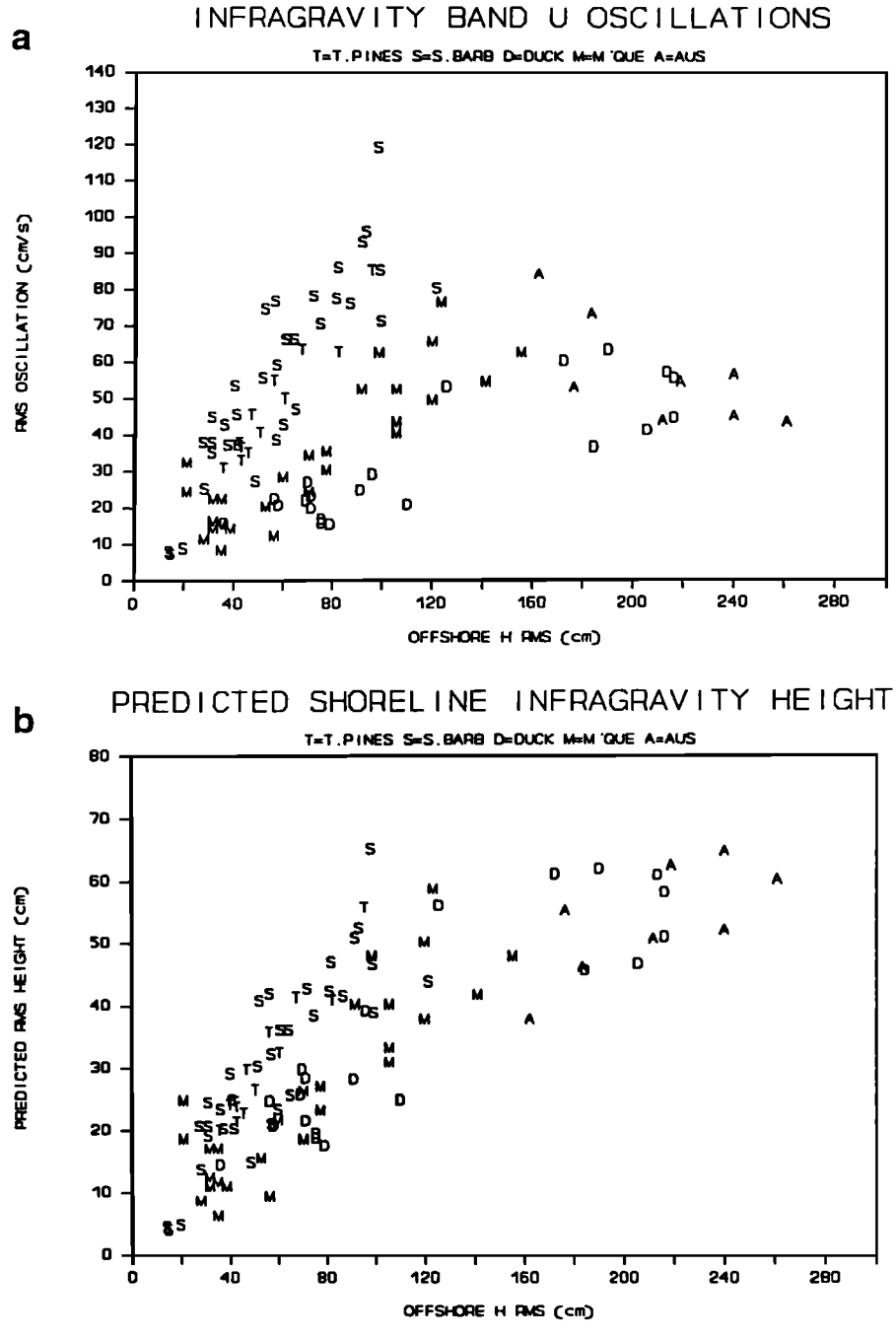

Fig. 11. (*a*) Comparison of u_{IG} oscillations from five beaches plotted versus the offshore wave height. There is considerable scatter in the data as a whole, yet each beach taken by itself is quite well behaved (Table 5). (*b*) The same data scaled to estimate the "equivalent shoreline height" $\hat{H}_{IG} = 2\hat{a}_{IG}$ of the infragravity oscillations (assuming a white spectrum). While the data collapse considerably, they are not statistically better correlated with offshore wave height at the 95% level (Table 5).

This approach is a particularly useful method to remove the site-specific nature of point measurements in the surf zone, thus facilitating the comparison of data collected either on different beaches, or at different cross-shore locations on the same beach.

While there is visual improvement in the clustering of the data (Figure 11*b*), the improvement in r^2 from 0.521 to 0.646 is not significant at the 95% level. This would seem to imply that to the lowest order, the magnitude of cross-shore infragravity oscillations are much less sensitive to the details of the incident wave spectrum or the beach topography than they are to the wave height. The lack of significant dependence on the cross-shore measurement location may be due to the limited range in dimensionless cross-shore space, $\chi = \sigma^2 x/g\beta$, for these measurements. There are indications (Figure 12), however, that there is a ξ_0 dependence for the regression slopes (equation (4)) in agreement with the prediction of *Holman and Sallenger* [1985] that infragravity energy levels depend on the Irabarren number.

It is important to note that these new measurements of infragravity and shear wave variances are representative of only one cross-shore distance, that of the array. It is clear that these results are influenced by the array location, since *Sallenger and Holman* [1985*a*] have shown u_{IG} to be a strong function of x on this same beach. The shear wave measurements, while clearly showing an important and energetic phenomenon, also need to be taken in the

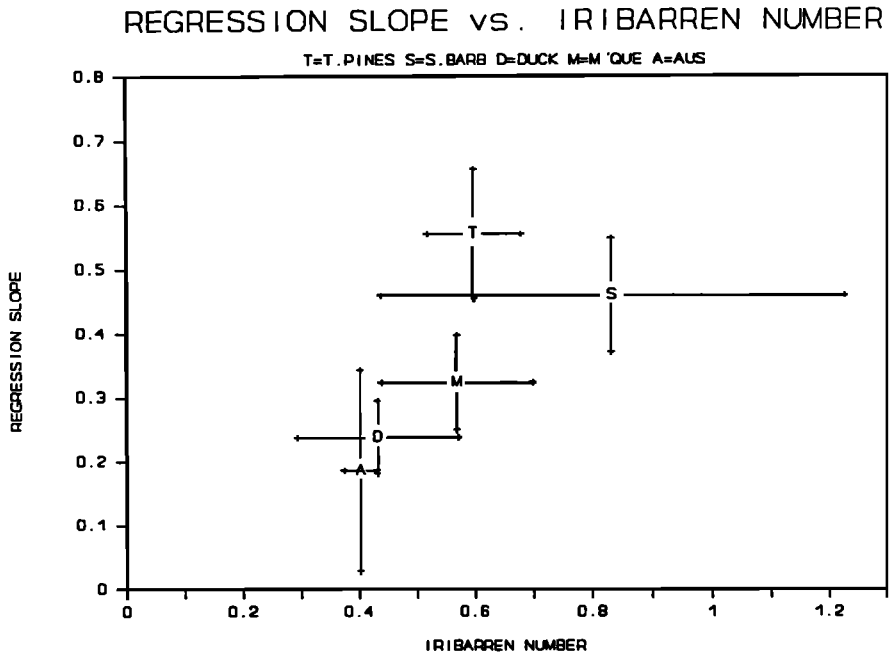

Fig. 12. Regression slopes for the five beaches (with 95% error bars) as a function of the mean Iribarren number (plus or minus one standard deviation) for that beach. There is a significant increase in regression slope with an increase in Iribarren number, confirming observations that infragravity waves tend to be larger on dissipative beaches than on reflective beaches for a given offshore wave height.

context of some (presently unknown) cross-shore variance structure. Recent measurements made during the 1990 DELILAH experiment should provide a clearer framework for understanding the cross-shore structure of these low-frequency motions.

Conclusions

Twenty-one 4-hour data runs collected over a wide range of incident wave conditions have been used to quantify the bulk statistical behaviors of the alongshore and cross-shore flow components of three classes of waves in the trough of a nearshore bar. The incident band oscillations, while not locally saturated, were limited by the presence of a depth minimum at the offshore bar. Thus the incident band, while not significantly correlated with the offshore wave height, was correlated with the tide elevation. The incident band at this location, approximately 55 m from the shoreline in the bar trough, is the largest contributor to total variance, typically providing 70–80%.

The infragravity wave oscillations averaged 20 cm s^{-1} and 32 cm s^{-1} for v_{IG} and u_{IG}, respectively, and are best parameterized by the offshore wave height. During storms they provided up to 33% of the total variance, with an average of approximately 12%. These percentages are expected to be higher at the shoreline. We have also found evidence that u_{IG}, the cross-shore component of infragravity wave oscillation, was, to a lesser degree, sensitive to the directional character of the incident waves.

Shear waves were found to be an important contributor to the energetics of this beach, typically comprising approximately 10% of the total variance, but at times contributing up to 35%. The magnitudes of the oscillations exceeded 40 cm s^{-1} in cross-shore and 30 cm s^{-1} alongshore. Shear wave magnitudes were correlated with the seaward facing shear of the longshore current (which was modeled, not measured), as expected from theory. It is difficult to place these measurements in cross-shore context with this data, owing to the lack of adequate measurement of the cross-shore structure of the longshore current.

Comparison of the cross-shore component of the infragravity band with data collected on other beaches and previously reported in the literature shows that while each experiment's data scales approximately linearly with offshore wave height, the trend of the relationship varies as a function of the Iribarren number. For these data, all collected in a similar depth of water, correcting for the cross-shore location of the sensor provides only a minor improvement in the correlation with the offshore wave height.

TABLE 6. Intercomparison of Beaches

Beach	$m \pm 95\%$ Confidence	b	r^2	DOF
*Surf-Zone u_{IG} rms Oscillations Versus Offshore Incident H**				
All beaches	0.174 ± 0.068	31.26	0.521	102
Torrey Pines	0.847 ± 0.153	0.24	0.924	11
Santa Barbara	0.839 ± 0.162	7.35	0.751	33
Duck	0.232 ± 0.027	7.80	0.776	19
Martinique	0.419 ± 0.095	3.73	0.759	25
Australia	−0.339 ± 0.315	127.69	0.479	6
*Equivalent Shoreline Height Versus Offshore Incident H**				
All beaches	0.215 ± 0.031	13.92	0.646	102
Torrey Pines	0.554 ± 0.100	0.15	0.924	11
Santa Barbara	0.459 ± 0.089	4.02	0.751	33
Duck	0.237 ± 0.057	7.77	0.790	19
Martinique	0.323 ± 0.073	2.87	0.759	25
Australia	0.185 ± 0.157	14.26	0.525	6

*Model: $u_{IG} = mH + b$ + error or equivalent shoreline height ($\hat{H}_{IG}$) = $mH + b$ + error.

Acknowledgments. We would like to thank (once again) the staff of CERC's Field Research Facility during the SUPERDUCK experiment. Not only did they assist whenever and wherever needed, they often did so without having to be asked. In addition to the manpower support, CERC

funded the deployment of the gages and the collection of the data which form the bulk of this paper. P.A.H. was employed by, and J.O.S. was under contract to, CERC during the period of the experiment. R.A.H. and the subsequent analysis of the data have been funded by grants from the National Science Foundation (OCE87-11121) and the Office of Naval Research, Coastal Sciences Program (N00014-87-K0009). This paper has been improved by the comments of Tony Bowen, Bob Guza, and the two anonymous reviewers.

REFERENCES

Birkemeier, W. A., and C. Mason, The CRAB: A unique nearshore surveying vehicle, *J. Surv. Eng., 110*, 1–7, 1984.

Bowen, A., D. Inman, and V. Simmons, Wave setdown and setup, *J. Geophys. Res., 37*, 206–215, 1968.

Bowen, A. J., and R. A. Holman, Shear instabilities of the mean longshore current, 1, Theory, *J. Geophys. Res., 94*, 18,023–18,030, 1989.

Crowson, R., W. Birkemeier, H. Klein, and H. Miller, SUPERDUCK nearshore processes experiment: Summary of studies CERC Field Research Facility, *U.S. Army Tech. Rep. CERC-88-12*, Coastal Eng. Res. Cent., Washington, D.C., 1988.

Eckart, C., Surface waves in water of variable depth, *Ref. 12*, 94 pp., Scripps Inst. of Oceanogr., La Jolla, Calif., 1951.

Elgar, S., and R. T. Guza, Observations of bispectra of shoaling surface gravity waves, *J. Fluid Mech., 161*, 425–448, 1985.

Elgar, S., J. Oltman-Shay, and P. Howd, Observations of infragravity-frequency long waves; I, Coupling to wind waves, *Eos Trans. AGU, 70*, 1333, 1989.

Galvin, C., and P. Eagleson, Experimental study of longshore currents on a plane beach, *U.S. Army CERC Tech. Memo. 10*, Coastal Eng. Res. Cent., Washington, D.C., 1965.

Guza, R., and A. Bowen, Resonant interactions for waves breaking on a beach, *Proc. Conf. Coastal Eng., 15th*, 560–579, Am. Soc. Civil Eng., New York, 1976.

Guza, R. and E. Thornton, Observations of surf beat, *J. Geophys. Res., 90*, 3161–3172, 1985.

Guza, R., E. Thornton, and R. Holman, Swash on steep and shallow beaches, *Proc. Conf. Coastal Eng., 19th*, 708–723, Am. Soc. Civil Eng., New York, 1985.

Haines, J., and A. J. Bowen, Phase-locking of modes in the nearshore: Field evidence, *Proc. Conf. Coastal Eng., 21st*, 1522–1534, Am. Soc. Civil Eng., New York, 1988.

Holman, R., Infragravity energy in the surf zone, *J. Geophys. Res., 86*, 6442–6450, 1981.

Holman, R., and A. Sallenger, Setup and swash on a natural beach, *J. Geophys. Res., 90*, 945–953, 1985.

Huntley, D., Evidence for phase coupling between edge wave modes, *J. Geophys. Res., 93*, 12,393–12,408, 1988.

Huntley, D., R. Guza, and E. Thornton, Field observations of surf beat, I, Progressive edge waves, *J. Geophys. Res., 86*, 6451–6466, 1981.

Kenyon, K., Edge waves with current shear, *J. Geophys. Res., 77*, 6599–6603, 1972.

Lippmann, T., The stability and spatial variability of sand bar morphology, M.S. thesis, 132 pp., Oreg. State Univ., Corvallis, 1989.

Longuet-Higgins, M., and R. Stewart, Radiation stress in water waves; A physical discussion, with applications, *Deep Sea Res., 11*, 529–562, 1964.

Oltman-Shay, J., and R. Guza, Infragravity edge wave observations on two California beaches, *J. Phys. Oceanogr., 17*, 644–663, 1987.

Oltman-Shay, J., P. Howd, and W. Birkemeier, Shear instabilities of the mean longshore current, 2, Field observations, J. Geophys. Res., 94, 18,031–18,042, 1989*a*.

Oltman-Shay, J., S. Elgar, and P. Howd, Observations of infragravity-frequency long waves, II, Comparisons with a 2-D wave group generation model, *Eos Trans. AGU, 70*, 1333, 1989*b*.

Pawka, S., Wave directional characteristics on a partially sheltered coast, Ph.D. dissertation, 246 pp. Scripps Inst. of Oceanog., Univ. of Calif., San Diego, 1982.

Pawka, S., Island shadows in wave directional spectra, *J. Geophys. Res., 88*, 2579–2591, 1983.

Sallenger, A., and R. Holman, On predicting infragravity energy in the surf zone, *Proc. Conf. Coastal Eng., 19th*, 1940–1951, Am. Soc. Civil Eng., New York, 1985*a*.

Sallenger, A., and R. Holman, Wave energy saturation on a natural beach of variable slope, *J. Geophys. Res., 90*, 11,939–11,944, 1985*b*.

Suhayda, J., Standing waves on beaches, *J. Geophys. Res., 79*, 3065–3071, 1974.

Thornton, E., and R. Guza, Energy saturation and phase speeds measured on a natural beach, *J. Geophys. Res., 87*, 9499–9508, 1982.

Thornton, E., and R. Guza, Surf zone currents and random waves: Field data and models, *J. Phys. Oceanogr., 16*, 1165–1178, 1986.

Weishar, L., and R. Byrne, Field study of breaking wave characteristics, *Proc. Conf. Coastal Eng., 16th*, 487–506, Am. Soc. Civil Eng., New York, 1978.

Wright, L. D., and A. D. Short, Morphodynamics of beaches and surf zones in Australia, in *CRC Handbook of Coastal Processes and Erosion*, edited by P. D. Komar, CRC Press, Boca Raton, Fla, 1983.

Wright, L. D., P. Nielsen, N. C. Shi, and J. H. List, Morphodynamics of a bar-trough surf zone, *Mar. Geol., 70*, 251–285, 1986.

R. A. Holman and P. A. Howd, College of Oceanography, Oregon State University, Oceanography Administration Building 104, Corvallis, OR 97331-5503.

J. Oltman-Shay, Quest Integrated, 21414 68th Avenue South, Kent, WA 98032.

(Received October 31, 1989;
accepted February 22, 1990.)